How to cite: *Angew. Chem. Int. Ed.* **2023**, *62*, e202310033
doi.org/10.1002/anie.202310033

VIP Metal-Organic Frameworks Very Important Paper

Bimetallic Anionic Organic Frameworks with Solid-State Cation Conduction for Charge Storage Applications

Yan Zhang, Jiande Wang, Petru Apostol, Darsi Rambabu, Alae Eddine Lakraychi, Xiaolong Guo, Xiaozhe Zhang, Xiaodong Lin, Shubhadeep Pal, Vasudeva Rao Bakuru, Xiaohua Chen,* and Alexandru Vlad**

Abstract: A new phosphonate-based anionic bimetallic organic framework, with the general formula of A_4–Zn–DOBDP (wherein A is Li^+ or Na^+, and $DOBDP^{6-}$ is the 2,5-dioxido-1,4-benzenediphosphate ligand) is prepared and characterized for energy storage applications. With four alkali cations per formula unit, the A_4–Zn–DOBDP MOF is found to be the first example of non-solvated cation conducting MOF with measured conductivities of 5.4×10^{-8} S cm^{-1} and 3.4×10^{-8} S cm^{-1} for Li_4- and Na_4- phases, indicating phase and composition effects of Li^+ and Na^+ shuttling through the channels. Three orders of magnitude increase in ionic conductivity is further attained upon solvation with propylene carbonate, placing this system among the best MOF ionic conductors at room temperature. As positive electrode material, Li_4–Zn–DOBDP delivers a specific capacity of 140 mAh g^{-1} at a high average discharge potential of 3.2 V (vs. Li^+/Li) with 90 % of capacity retention over 100 cycles. The significance of this research extends from the development of a new family of electroactive phosphonate-based MOFs with inherent ionic conductivity and reversible cation storage, to providing elementary insights into the development of highly sought yet still evasive MOFs with mixed-ion and electron conduction for energy storage applications.

[*] Y. Zhang, X. Chen
College of Materials Science and Engineering, Hunan Province Key Laboratory for Advanced Carbon Materials and Applied Technology, Hunan University
Changsha 410082, Hunan (P. R. China)
E-mail: xiaohuachen@hnu.edu.cn

Y. Zhang, J. Wang, P. Apostol, D. Rambabu, A. Eddine Lakraychi, X. Guo, X. Zhang, X. Lin, S. Pal, V. Rao Bakuru, A. Vlad
Institute of Condensed Matter and Nanosciences, Université catholique de Louvain
1348 Louvain-la-Neuve (Belgium)
E-mail: jiande.wang@uclouvain.be
alexandru.vlad@uclouvain.be

Introduction

The recent increasing concerns on the performance bottlenecks and the environmental footprint of current Li-ion batteries technology, have pushed researchers to seek and develop various alternative energy sources and methods, with organic-based chemistries emerging as a particular class to tackle in particular the sustainability aspects.[1] Metal–organic frameworks (MOFs) have attracted special attention as active electrode materials, or as electrode additives due to their structural tunability, post-synthetic functionality, conductivity (ionic or electronic), porosity, or surface area, as well as the richness of fundamental science provided by merging the electrochemical science and coordination chemistry in a solid porous framework.[2] As active charge storage materials, MOFs can be divided into three categories according to the nature of the active redox center: reversible redox of metal,[3] of the ligand,[4] or more appealing, mixed redox of both.[5] Important to note, most MOFs reported so far have been prepared in their oxidized state, and thus used either as negative electrode material (i.e. negative electrode of a Li-ion cell), or at best as moderate voltage positive electrode material for Li-metal cells.[6] To be used as Li-ion positive electrode materials, these should either be directly synthesized in the reduced Li-ion containing form, or require coupling to lithiated negative electrode materials. The former option is particularly interesting from a fundamental viewpoint as it can be considered as a bimetallic MOF. The nature (redox, non-redox, monovalent, divalent) and coordination environment (as part of the secondary building unit and potentially with extremely low mobility compared to freely attached ions) of the different metal cations have the potential to influence the electrochemical and physicochemical properties of the respective MOFs. This variation in properties is especially significant when considering the frustrated coordination environment, which may enable higher mobility of the metal cations.

The ionic and electronic conductivity of MOFs can have in fact a critical impact on the performances for many applications, including in energy storage devices, electrolysers, or electrocatalysts. MOFs have been suggested to possess unique tuneable chemical and structural properties, which could enable facile electron and ion transport.[7] While the electrical conductivity has been extensively explored and reported, especially in 2D MOFs,[8] the number of MOFs with ionic conductivity remains limited to date. The main

challenge in designing ionic conductive MOFs is to introduce an anionic functionality that will bind weakly to the ionic carriers, such as Li-ions. Considering the charge neutrality, the methodology for the introduction of cations can be classified into two approaches: inclusion of salts into the MOF framework, or exchange of protons or counter cations of an anionic-lattice MOFs with the desired ions (e.g. Li^+, Na^+ etc).[9] Whereas both methods have been applied and revealed successful in synthesis, efficient dissociation of cation from guest salt, or from anionic framework remains challenging. For example, Wiers et al. reported the incorporation of LiOiPr and $LiBF_4$ salts with guest solvents such as ethylene carbonate and diethyl carbonate in Mg_2-DOBDC (Mg–CPO-27) structure to attain a Li^+ conduction of 3.1×10^{-4} S cm^{-1} at 300 K.[10] Park et al. reported another example of lithium-ion conductive MOF after introducing LiCl, LiBr, or $LiBF_4$ within a [Cu_2Cl_3BTDD] framework, with conductivity values attaining 10^{-4}–10^{-5} S cm^{-1} at 298 K, yet, measured in presence of propylene carbonate (PC) solvent.[7b]

Alternatively, the ion exchange technique was employed to modify the anionic MOF-688 framework, where NBu^{4+} cations were replaced with Li^+. In order to promote effective dissociation of Li-ions from the framework (which consists of an Anderson-type polyoxometalate) and thus enhance the ionic transport, the Li-MOF-688 was also infiltrated with PC. This resulted in the formation of a quasi-solid MOF Li-ion conductor, exhibiting an ionic conductivity of 3.4×10^{-4} S cm^{-1} at 293 K.[11] From an overview of the field, it is straightforwardly clear that ionic conduction in MOF has been attained so far mainly upon cation solvation.[12] However, the inclusion of solvents in ion-conducting MOFs, particularly for Li-ion systems, has sparked a controversial debate regarding their classification as either true solid-state conductors, or conductors resembling polymer gels, characterized by solvent-soaked molecular structures facilitating cation transport. Achieving genuine solid-state conduction in MOFs thus remains an intriguing scientific curiosity and a practical challenge. It is worth noting that the commonly assigned porosity for facilitating transport in MOFs may not be universally valid, since the most efficient ionic conductors discovered thus far exhibit compact and dense structures.[13] Consequently, a distinct design rationale is required in terms of structural and compositional aspects to enable true solid-state ionic conduction in MOFs.[14]

Herein, we report on the synthesis and properties of Li- and Na-ion containing anionic MOFs, with the empirical formula: A_4–Zn–DOBDP (A=Li^+ or Na^+, $DOBDP^{6-}$ = 2,5-dioxido-1,4-benzenediphosphate), displaying true solid-state ionic conduction as well as reversible redox - key properties for advanced energy storage systems. The A_4–Zn–DOBDP MOF is synthesized by post-synthetic proton-cation exchange of desolvated H_4–Zn–DOBDP MOF. The deprotonated A_4–Zn–DOBDP MOFs was found to exhibit Li-ion and Na-ion conductivities of 5.4×10^{-8} and 3.4×10^{-8} S cm^{-1} at 303 K, respectively, placing these phases as the highest (and to the best of our knowledge, the only reported) true solid-state alkali-ion conductor MOFs. A factor of 3-fold magnitude increase in conductivity is gained in a quasi-solid-state phase configuration, upon impregnation and solvation of the A_4–Zn–DOBDP MOF with PC. As an alkali-ion containing positive electrode material, Li_4–Zn–DOBDP displays a specific reversible capacity of 140 mAh g^{-1} at a high average discharge redox potential of 3.2 V vs. Li^+/Li, with stable cycling stability performances. The capacity and voltage are also among the highest in Li-ion containing MOFs so far, representing a significant step towards the practical application of organic or metal-organic materials in batteries.

Results and Discussion

Recent efforts focusing on the development of *n*-type alkali cation containing MOF positive electrode materials, that possess the properties of conventional inorganic Li/Na-ion materials have provided significant results. For instance, the initial report of Mg(Li_2)-*p*-DOBDC (magnesium [2,5-dilithium-oxy]-terephthalate) reported by Poizot et al. enabled a reversible capacity of 100 mAh g^{-1} at redox potential of 3.4 V vs. Li^+/Li, due to the high ionic potential of Mg^{2+}.[15] Shortly after, another two Li-containing MOFs, Li_2-(Mg/Mn)–DOBDC, were reported as the first Li-ion containing MOF positive electrode materials for batteries, with intrinsic electron conductivity of the Mn^{2+} phase of the order of 10^{-7} S cm^{-1}, and a practically high average discharge potential of 3.2 V vs Li^+/Li. However, and counterintuitive, despite being a Li-ion rich MOF composition, the Li_2-(Mg/Mn)–DOBDC phases displayed no ionic conductivity (below the measurement resolution limit of 10^{-12} S cm^{-1} at 70 °C).[6e] It was thus hypothesized that strong ionic binding of Li^+ to the enolate O^- group blocks the ionic mobility, despite the high density of charge carriers present in the MOF channels (2 Li^+ per formula unit). Additionally, due to the low anodic stability of the used ligand ($DOBDC^{4-}$ - 2,5-dioxido-1,4- benzenedicarboxylate), a low reversible capacity of 60 mAh g^{-1} was attained (one electron limited redox of the organic unit),[6e] which may limit its practical application. Important to note, the Li_2–Mg–DOBDC as a polymorph of Mg(Li_2)-*p*-DHT (magnesium [2,5-dilithium-oxy]-terephthalate) displayed different electrochemical properties; whereas Li_2–Mn–DOBDC, displayed additionally intrinsic electrical conductivity, a highly interesting feature for electrochemical energy storage.[6e,15]

Afterwards, electrically conducting Li-ion containing coordination polymers have been reported by Wang et al., which also exhibited the appealing property of a high average discharge potential around 3.0 V (vs. Li^+/Li), alongside with a reversible capacity of 100 mAh g^{-1}.[6d] This class of coordination polymers also has the potential of metal redox centered charge storage, which could result in a higher capacity, if excess alkali cations are available. In fact, all above mentioned systems, are 2-electrons and 2-Li^+ limited, as either the redox is limited to 2 electrons, or if more than 3 electron redox is possible (for instance, by adding the redox of a transition metal), the limited Li^+ content will either block the redox, or enable anion storage (as in p-type

systems). Thus, if one desires to design Li-cation rich systems, a different rationale is required.

According to the above-mentioned design criteria and limitations, we hypothesized that a hexa-anionic linker (instead of tetra-anionic as earlier discussed) would be most suitable to allow the design of cation-rich (Li^+, or Na^+) system. If the composition and topology can be precisely tailored, in that a divalent metal cation could bind to the hexa-anionic linker in a 1:1 stoichiometric ratio, the charge balance will formally require four additional mono valent cations (or protons, H^+). Since hexa-anionic organic ligands, that would also display a reversible redox (as per our interest in charge storage applications) are quite rare, we have selected an intriguing hydroquinone derivative, the 2,5-dihydroxy-1,4-benzenediphosphonic acid (H_6–DOBDP), for the development of Li/Na-rich MOFs. The hexa-anionic nature of H_6–DOBDP is particularly interesting, as all 6 protons (one per each hydroxy, and two per each phosphonate groups) are acidic, and can be thus replaced if an adequate base is used. The incorporation of $DOBDP^{6-}$ into a MOF structure is also expected to enhance the electrochemical performances due to the structural rigidity and facile solvated ion diffusion in the porous structure.

The H_4–Zn–DOBDP MOF has been thus selected due to the simple synthetic procedure and the target stoichiometry of 1-to-1 between Zn^{2+} and $DOBDP^{6-}$, with thus attaining the target composition of $(H/Li/Na)_4$–Zn–DOBDP being conceptually possible. The synthesis of H_4–Zn–DOBDP MOF was achieved by considering previously reported protocol with some modifications (refer to Figure S1 and Experimental Section in Supporting Information).[16] The as-synthesized MOF, H_4–Zn–DOBDP·2DMF has a three-dimensional microporous structure (as determined from single crystal, as well as PXRD data) with Zn^{2+} centers binding adjacent linkers (Figure 1B and S1). The SBU is formed by the Zn^{2+} nodes tetrahedrally coordinated by four O atoms of four different phosphonate groups (Figure 1B and 1C). The phosphonate groups act as bidentate ligand, bridging two Zn^{2+} nodes, forming 1D chains along the *c*-axis (Figure 1B), extending in 3D space by interlinking the phenyl spacer of H_4–$DOBDP^{2-}$. The rhombohedral micropores (10.4 Å×10.4 Å) along *c*-axis accommodate DMF molecules (Figure 1B and S1A). The MOF also has ultra-micropores along the *b*-axis with a narrow point of 4.3 Å (Figure S1B).

There are several peculiar features of the pristine H_4–Zn–DOBDP MOF that motivated us to undertake the proton by alkali cation replacement, analyse the ion diffusion properties, as well as test the reversibility of the two-electron redox of the quinone-dioxidobenzene redox unit. First, the DMF molecules accommodated in the pores as host–guest interactions, are not involved in the framework formation, making them removable under mild processing conditions. This is important to the desolvation

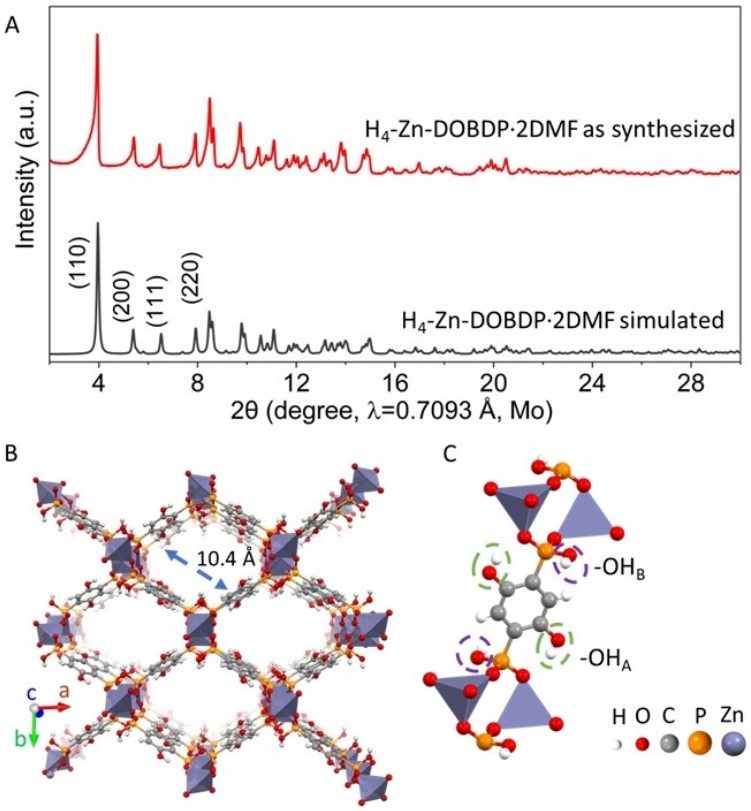

Figure 1. PXRD pattern (A) and crystal structure illustration of H_4–Zn–DOBDP·2DMF MOF (B). DMF molecules are omitted for clarity highlighting the pore size. (C) Zoom in image of the ligand highlighting the presence of two different types of accessible hydroxy groups: phenolic ($–OH_A$) and phosphonate ($–OH_B$) hydroxy groups.

process, and essential for subsequent functionalization, in that it can be performed without compromising the framework lattice structure. Second, the two phenolic hydroxy groups ($-OH_A$) pointing inside the pores along the *c*-axis (Figure S1B) and the two hydroxy ($-OH_B$) groups, one from each phosphonic group, remain accessible. According to previous work by Rambabu et al., it has been shown that in order to preserve the redox activity of phenolates, these should not bind to primary metal cation (herein Zn^{2+}) involved in the MOF structure formation.[6e] The main interest in H_4–Zn–DOBDP MOF is thus the fact that the phenolates are free and cannot coordinate to Zn^{2+} during the post synthetic modification step given that the Zn^{2+} has already the coordination environment saturated. Moreover, the topology of H_4–Zn–DOBDP nearly resembles the one of H_2-(Mg/Mn)–DOBDC with anionic functionality (Figure 1B, 1C and S1A).

The topotactic reversible conversion of H_4–Zn–DOBDP·2DMF to A_4–Zn–DOBDP (A=Li^+, and Na^+) phase was performed in two steps, as schematized in Figure 2A. The first step involves the desolvation of H_4–Zn–DOBDP·2DMF that empties the pores and potentially enables faster reactants diffusion for proton-cation exchange. Upon heating of H_4–Zn–DOBDP·2DMF, a 30 % weight loss in the range 160–180 °C was detected from TGA (Figure S3), attributed to the complete desolvation of the MOF. This process is accompanied by a pronounced color change from white to light brown (Figure 2A). The complete DMF removal was also confirmed by the disappearance of C=O stretching vibration ($\approx$1600 cm^{-1}) of DMF (Figure 2B) in FTIR analysis. The broad –OH ($-OH_A$ and $-OH_B$) band positioned around $\approx$3450 cm^{-1} remains preserved after activation, (Figure 2B), suggesting structural robustness of H_4–Zn–DOBDP during thermal treatment. The shift to higher wavenumbers of the O–H band in H_4–Zn–DOBDP as compared to H_4–Zn–DOBDP·2DMF can be interpreted as follows: in the solvated framework of H_4–Zn–DOBDP·2DMF, the C=O groups of DMF engage in hydrogen bonding interactions with phosphonate O–H_B groups. However, upon desolvation, these interactions are lost, leading to an increase in the strength of the O–H_B bonds, thus resulting in a shift to higher wavenumbers. Powder X-ray diffraction (PXRD) revealed a phase change upon desolvation accompanied by a shift of the low-angle peaks from 2θ = 3.9°, 5.4° and 6.5° to 2θ = 4.6°, 5.0° and 6.1°, respectively, suggesting the preservation of the open framework albeit minor shrinking and lattice distortion (Figure 2C). Impregnation of the H_4–Zn–DOBDP with DMF, resulted in the reformation of initial solvated phase (marked as H_4–Zn–DOBDP_DMF), evidenced by both FTIR and PXRD data (Figure 2B and 2C), indicating pore accessibility, the reversibility of the desolvation/solvation process and stimuli-flexible[17] nature of the H_4–Zn–DOBDP framework upon solvent exchange.

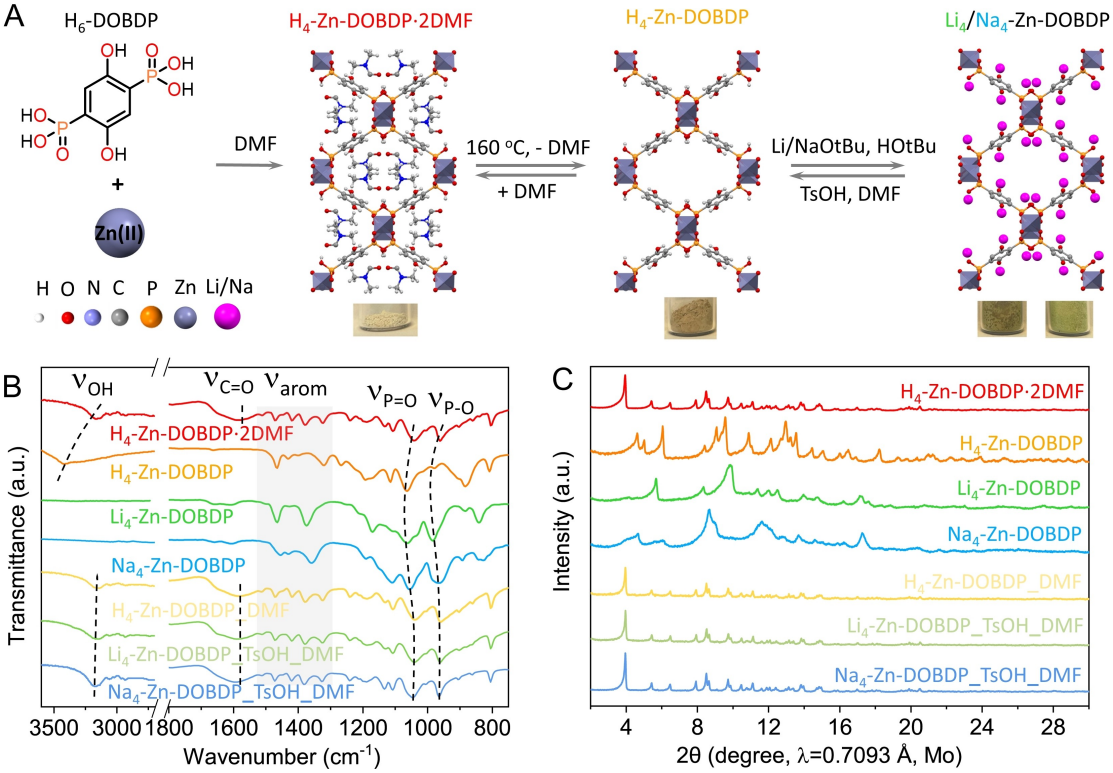

Figure 2. (A) Schematic illustration of the synthetic route adopted for target compounds, H_4–Zn–DOBDP 2DMF, Li_4–Zn–DOBDP and Na_4–Zn–DOBDP, highlighting the reversibility of the last two steps. Bottom insets: photos of the respectively synthesized powder form materials. Overlaid FTIR spectra (B) and powder XRD patterns (C) of target compounds as well as of intermediate phases obtained during the post-synthetic desolvation (H_4–Zn–DOBDP) and cation exchange (Li_4–Zn–DOBDP and Na_4–Zn–DOBDP).

The deprotonation step however revealed to be more challenging than compared to previous similar developments (i.e. with Mg(Li_2)-*p*-DHT,[15] or Li_2-(Mg/Mn)–DOBDC[6e]). For instance, by using lithium hydride (dispersed in DMF), lithium methoxide (solution in methanol), lithium diisopropylamide (dispersed in THF/hexane), and lithium tert-butoxide (LiOtBu, solution in tert-butyl alcohol) at room temperature, full deprotonation and lithiation of H_4–Zn–DOBDP was not possible, resulting in phases containing partially protonated ligands (refer to Figure S4 and Table S1 for additional details and discussion). Quantitative deprotonation of H_4–Zn–DOBDP, yielding the tetra-anionic Zn–$DOBDP^{4-}$, was attained only under refluxing conditions while using LiOtBu or NaOtBu in tert-butyl alcohol (Figure 2B), leading to Li_4–Zn–DOBDP and Na_4–Zn–DOBDP, respectively. One plausible explanation could be that the re-solvation and pore clogging results in slower reactant mass transfer for the reaction to complete at room temperature, although further studies might be required to clearly understand these limitations. The complete lithiation (or sodiation) was confirmed by the disappearance of the phenolic $–OH_A$ and phosphonic $–OH_B$ band at 3450 cm^{-1}, accompanied by colour change from light brown to green (Figure 2A and 2B). The inductively coupled plasma atomic emission spectroscopy (ICP-AES) and X-ray Fluorescence Spectroscopy (XRF) analysis revealed close to expected compositions of 1 : 4.01 mol.eq. (or atomic ratio of Zn : Li) for Li_4–Zn–DOBDP and 1 : 3.75 mol.eq. (Zn: Na) for Na_4–Zn–DOBDP. The morphology of Li_4–Zn–DOBDP and Na_4–Zn–DOBDP powders was also investigated by SEM and TEM (Figures S5 and S6), revealing that both materials are made of 1 μm particles, comparable in size and shape to H_4–Zn–DOBDP·2DMF and H_4–Zn–DOBDP pristine materials.

Cation exchange within MOFs via post-synthetic modification is a well-acknowledged process, and the current work makes no exception to this. For instance, the introduction of alkali cations may also compete and exchange with Zn^{2+} and potentially cause the collapse and degradation of the MOF structure. As illustrated in Figure 2C, the framework indeed undergoes significant structural changes after H^+/Li^+ or H^+/Na^+ exchange, with also different phases obtained between Li_4- and Na_4- compositions. The poor crystallinity of the Li_4- and Na_4- phases was however insufficient for crystal structure refinement and precluded us to provide unambiguous evidence for the preservation of the framework. Thus, an indirect method of re-protonation and re-solvation was adopted, wherein the Li_4–Zn–DOBDP and Na_4–Zn–DOBDP materials were treated with four equivalents of *p*-Toluenesulfonic acid (TsOH) in DMF. As shown in Figure 2B and 2C, the re-protonated and re-solvated phases (Li_4/Na_4–Zn–DOBDP_TsOH_DMF) show identical PXRD and FTIR spectra to the pristine H_4–Zn–DOBDP·2DMF phase, proving the chemical and structural reversibility and stability of the MOFs. Therefore, it is reasonable to conclude that the coordination environment of Zn^{2+} is insignificantly affected, and the structure of H_4–Zn–DOBDP·2DMF MOFs is perserved throughout the entire process.

The alkali-ion conduction property of A_4–Zn–DOBDP MOS was next assessed, considering the particular structure and composition of these phases: high alkali-ion content (four alkali-ions per formula unit), two different binding sites ($–O[H/A]_A$ and $–O[H/A]_B$, Figure 1C), with thus also different binding energy and coordination frustration, that are expected to impact the ion conduction. The proton and ion conductivity measurements for H_4–Zn–DOBDP·2DMF and A_4–Zn–DOBDP were performed on both, desolvated (i.e. true solid-state conduction) as well as solvated phases, with finite measurable values for both, and a comparison being made. To recall, known reports on alkali-ion conducting MOF phases are based on either immobilization of anions at the unsaturated metal sites to induce cation-anion dissociation,[7c] or ion-proton exchange in anionic frameworks.[18] Essential, all the materials should be considered as quasi-solid ionic conductors, since residual solvent or electrolyte soaking was always necessary to activate the ion conduction (most certainly given the strong cation-anion binding, with thus screened interaction upon cation solvation).[10,19] Since the true solid phase ionic conduction in MOF remains elusive to date, to the best of our knowledge, the A_4–Zn–DOBDP (A=Li or Na) phases studied in this work are the first examples of pure MOF-based solid conductors.

Figure 3A displays the Nyquist plots of pristine H_4–Zn–DOBDP·2DMF as well as of dry and solvated A_4–Zn–DOBDP phases measured at 303 K. All exhibit a high frequency semicircle and a low frequency linear response, also measured at different temperatures (Figure 3A and Figure S7). Usually, the latter is associated to the blocking effect at electrode and is typical of proton/ionic conductor behavior. Fitting the results of PEIS to the circuit gave $H^+/Li^+/Na^+$ conductivities of 9.3×10^{-8}, 5.4×10^{-8} and 3.4×10^{-8} S cm^{-1} at 303 K for H_4–Zn–DOBDP·2DMF, Li_4–Zn–DOBDP (dry) and Na_4–Zn–DOBDP (dry), respectively (Table 1). Generally, the cation transport in MOFs can be explained by two mechanisms: 1) anionic site hopping, by which the ions migrate from one anionic site (or biding-coordination sites) to another, and 2) solvent hopping, by which ions are transfered from one bridging solvent molecule to another.[7b,c,9,20] The former mechanism remains however less understood, and is generally associated to high defect, carrier concentration and short hopping distance. Binding energy and coordination environment (or frustrated

Table 1: Proton conductivity, ionic conductivity, and activation energy of H_4–Zn–DOBDP·2DMF, A_4–Zn–DOBDP and A_4–Zn–DOBDP_PC. (A=Li/Na) phases.

Sample	σ [S cm^{-1}][a]	E_a [eV][b]
H_4–Zn–DOBDP·2DMF	9.3×10^{-8}	0.09
Li_4–Zn–DOBDP	5.4×10^{-8}	0.23
Na_4–Zn–DOBDP	3.4×10^{-8}	0.24
Li_4–Zn–DOBDP_PC (22 wt.%)	2.7×10^{-5}	0.16
Na_4–Zn–DOBDP_PC (16 wt.%)	1.1×10^{-6}	0.20

[a] Proton and ionic conductivity (H^+, Li^+ and Na^+) at 303 K. [b] Activation energy.

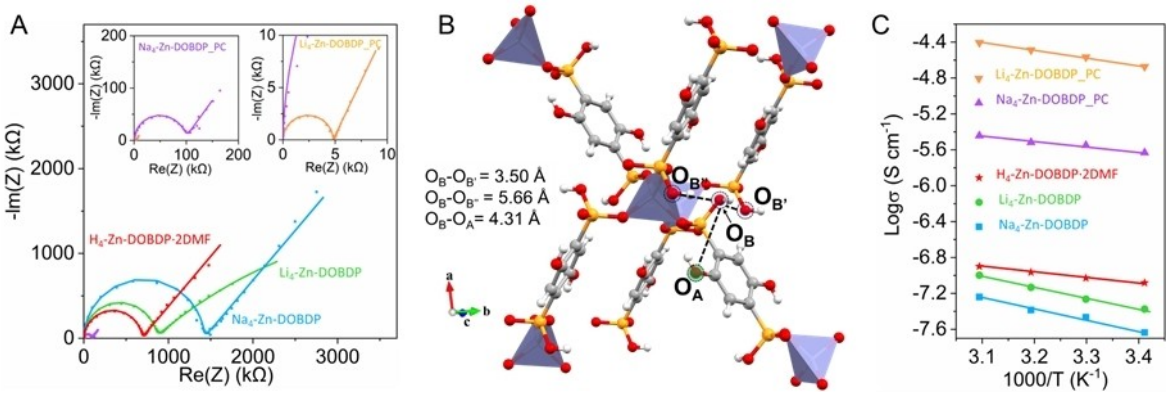

Figure 3. Proton and ionic conductivity analysis of H_4–Zn–DOBDP·2DMF as well as of solvated and solid-state A_4–Zn–DOBDP (A=Li and Na) phases. (A) Nyquist plots of H_4–Zn–DOBDP·2DMF, Li_4–Zn–DOBDP, Na_4–Zn–DOBDP, Li_4–Zn–DOBDP_PC and Na_4–Zn–DOBDP_PC at 303 K. The solid line represents the best fit to experimental data. (B) Structural representation of H_4–Zn–DOBDP·2DMF highlighting the different anionic sites and the distance between these. (C) Temperature dependence of the proton and ionic conductivity of the studied materials and phases.

environment) are of additional importance, as these dictated the activation energy for site-to-site migration.

The A_4–Zn–DOBDP phases contain adequate Li^+/Na^+ hopping sites, with four anionic sites per ligand. Notably, the short distance between hopping sites as well as the low binding energy of cations and anionic framework endows A_4–Zn–DOBDP with promising ionic conduction properties. According to the crystal structure of H_4–Zn–DOBDP·2DMF (Figure 3B), the closest distance between phosphonate and phenolate oxygen atoms is O_B–O_A = 4.31 Å, with the two oxygens from the same ligand, while the two phosphonate oxygen atoms along the pore direction (c axis) is much shorter (O_B–$O_{B'}$ = 3.50 Å). Considering the reversible structure modification during desolvation and proton exchange by Li^+/Na^+ and stable tetrahedral coordination environment for Zn^{2+} it can be assumed that the phosphonate oxygen atoms and phenolic ones remain in vicinity, facilitating the ionic conduction via energy favorable hopping transfer mechanism. In addition, the phosphonic acid functionality generally has the first pKa ranging from 1.1 to 2.3 and the second ranging from 5.3 to 7.2, which are much lower than of the phenols (pKa > 10).[21] The higher acidity of phosphonic acid also indicates lower binding energy of a phosphonate anion with a proton or with a cation, so that the cations residing in the phosphonate sites are potentially more mobile. When compared to Li_2-(Mg/Mn)–DOBDC,[6e] with only the phenolate anionic sites on the ligand, the stronger binding energy between phenolate and Li^+ inhibits the ionic transport, leading to no measurable ionic conductivity. Therefore, it is reasonable to conclude that the major Li^+/Na^+ transport in A_4–Zn–DOBDP dry solid is the hopping through phosphonate anionic sites.

The ionic conductivity of Li_4–Zn–DOBDP was also found to be slightly higher than that of Na_4–Zn–DOBDP (Figure 3A and 3C). Although a relatively smaller ionic radius of Li^+ than Na^+ can lead to smaller steric hindrance, the larger ionic radius (Na^+) should also lower the dissociation energy, and thus enable faster cation transport. The trade-off certainly requires more investigation to understand and explain this phenomenon, while also taking into account the significant phase changes between both, Li_4- and Na_4- phases, with thus a direct comparison being not strictly adequate.

Interestingly, the solvated H_4–Zn–DOBDP·2DMF exhibits a proton conductivity of 9.3×10^{-8} S cm^{-1} at a temperature of 303 K, and under 0% RH conditions. However, when the MOF was desolvated (DMF removed), no proton conduction was possible to measure. This absence of proton conduction can be attributed to the disappearance of hydrogen bonding interactions (specifically, proton-oxygen-hydrogen bonding with the solvent DMF) and the formation of stronger oxygen-hydrogen bonds. This conclusion is supported by FTIR analysis, which reveals a shift towards higher wavenumbers in the bond frequencies upon desolvation, indicative of the establishment of stronger O–H bonds (Figure 2B).

To be noted that in absolute, the solid-state ionic conduction of Li/Na_4–Zn–DOBDP phases may be considered as modest when compared to state-of-the-art Li- and Na-ion conducting systems. Nevertheless, from a fundamental point of view, attaining non solvated cation transport in MOF represents a significant milestone for understanding and designing better ion conducting MOF materials. Although certainly this may represent a limitation for a solid-state cell device design (along with also low electronic conductivity of these phases), this may not be the case in a liquid electrolyte-based cell, as solvation could take place, as confirmed by the post-functionalization reversibility analysis discussed earlier (Figure 2). To test this, we have also measured the ionic conductivity of the Li$_4$/Na$_4$–Zn–DOBDP phases after adding a controlled amount of propylene carbonate (PC) to solvate the cations, a feature uniquely available in MOFs given the open framework structure of these materials (Figure 3A and 3C). The PC solvated Li_4–Zn–DOBDP and Na_4–Zn–DOBDP MOFs were found indeed to display three orders magnitude increase in conductivity (in the range of 10^{-5}–10^{-6} S cm^{-1}, Figure 3C,

Table 1 and Table S3). The cation conductivity is thus clearly enhanced by solvation shell charge screening, and dominated by solvent assisted hopping, with the rate of this process depending on the solvation-desolvation energy. Interestingly, solvated Li_4–Zn–DOBDP displays one order magnitude higher ionic conductivity than solvated Na_4–Zn–DOBDP, indicating that the pore size in A_4–Zn–DOBDP is playing an important role in solvated phase, by limiting the Na^+ transport due to its much bigger size. To ascertain the influence of the pore environment and cation identity on conductivity, we determined the activation energy for ion transport by collecting variable-temperature impedance data between 293 K and 323 K, showing a low activation energy in the 0.16–0.25 eV range (Table 1), in line with the values found to other solvated MOF ionic conductors.[7b,c] The low activation energy also suggest that the efficient conducting pathways for the Li^+/Na^+ carrier are formed inside the channels of Zn–DOBDP MOFs. Another interesting aspect to be mentioned is the differences along with the similarity in activation energies between the dry and solvated phases. For instance, whereas the absolute conductivity values show significant difference, the activation energies are nearly similar between the solvated (0.16, 0.20 eV) vs unsolvated (0.23, 0.24 eV) phases, further confirming that the ion transport mechanism are different between these.

The electrochemical performance of A_4–Zn–DOBDP as positive electrode material was next investigated for both, Li- and Na- ion storage (Figure 4, and Figure S13 for Na_4–Zn–DOBDP/Na). Upon charge (corresponding to delithiation) of Li_4–Zn–DOBDP at a rate of 0.1 C (equivalent of 1 electron exchange in 5 h), a slopped plateau averaging at 3.2 V vs. Li^+/Li was revealed, with a specific capacity of 140 mAh g^{-1} at the end of the process (corresponding to 1.86 Li^+/e^- per formula unit exchange, Figure 4A). The corresponding discharge (lithiation) shows high electrochemical reversibility with a high initial coulombic efficiency of 95 %. Due to the good ionic conductivity of the solvated phase, Li_4–Zn–DOBDP also shows competitive rate performances, with nearly 90 mAh g^{-1} being retained at a high charge–discharge rate of 1 C. The cell also displays good cycling stability, with nearly 90 % of capacity retention attained at a rate of 0.1 C for 100 cycles (over a period of 2 months testing, Figure 4C). Even at 2 C, Li_4–Zn–DOBDP retains 71 mAh g^{-1} after 200 cycles accompanied by high average coulombic efficiency (99.6 %, Figure S9). The excellent cycling stability is first of all attributed to the structural rigidity and the insoluble nature of the polymeric type Li_4–Zn–DOBDP MOF. Another essential feature of

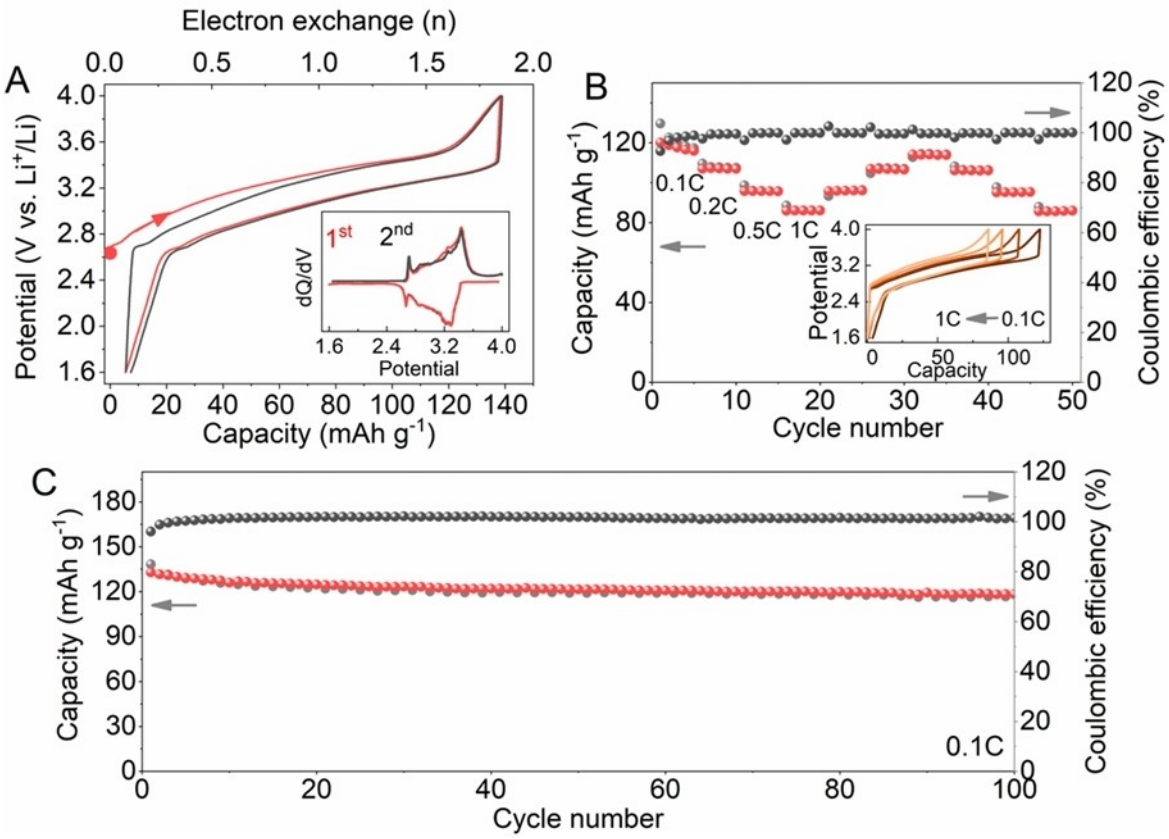

Figure 4. Electrochemical performance of Li_4–Zn–DOBDP electrode material. (A) Gavlanostatic charge–discharge profiles of the first two cycle voltage profiles at a C-rate of 0.1, the inset is the corresponding differential capacity plot as a function of Potential (dQ/dV vs E). (B) Rate capability performance test. The inset shows the voltage-capacity profiles corresponding to the used C-rates from 0.1 C to 1 C. (C) Long-term cycling performance attained at a cycling rate of 0.1 C.

the disclosed A_4–Zn–DOBDP MOFs is that although the OCV is slightly lower than the air stability limit value of ≈2.91 V vs. Li^+/Li, the A_4–Zn–DOBDP phases show good ambient air and water stability, an important asset for handling and processing of the electrode materials in ambient air. Chemical and electrochemical analyses of the air-exposed powders displayed minimal oxidation, with the battery galvanostatic charge–discharge profile showing slightly lower capacity in the first charge but highly reversible behaviour in the subsequent cycles (Figure S10–S12).

Conclusion

The remarkable flexibility exhibited by H_4–Zn–DOBDP 2DMF allows for a reversible phase transition between protonated and cation rich Li_4/Na_4–Zn–DOBDP phases. The approach introduced in this study involves accessing a negatively charged framework through post-synthetic modification of the MOF. This is achieved by replacing the labile hydrogen atoms of the ligand's hydroxy and phosphonate groups with desired alkali metal ions. The prepared Li- and Na-ion rich MOFs demonstrate the characteristics of true solid-state ionic conductors, and are amongst the first examples of non-solvated cation transport in a porous framework. At a temperature of 303 K, the Li_4- and Na_4-phases exhibit ionic conductivities of 5.4×10^{-8} S cm^{-1} and 3.4×10^{-8} S cm^{-1}, respectively; with 3 orders of magnitude gain in conductivity attained upon cation solvation. Overall, the comprehensive study on A_4–Zn–DOBDP not only provides valuable guidelines to explore phosphonate MOFs for ionic conductivity applications but also inspire and pave way for the development of alkali-cation containing organic cathode materials for future battery technologies.

Supporting Information

Supporting Information is available from the Wiley Online Library or from the author.

Acknowledgements

Y.Z., J.W., X.G. and X.Z. acknowledge China Scholarship Council for the funding support. D.R. acknowledges F.R.S.-FNRS for the Chargé de Recherché fellowship (grant agreement No. 40010410). X.L. acknowledges MSCA fellowship (grant agreement No. 101064286). A.V. is indebted to the European Research Council under the European Union's Horizon 2020 research and innovation program (grant agreement No. 770870, MOOiRE).

Conflict of Interest

The authors declare no conflict of interest.

Data Availability Statement

The data that support the findings of this study are available from the corresponding author upon reasonable request.

Keywords: Alkali Ion Storage · High Voltage · Ionic Conduction · Metal–Organic Framework · Organic Battery

[1] a) J. Li, J. Fleetwood, W. B. Hawley, W. Kays, *Chem. Rev.* **2022**, *122*, 903; b) A. Vlad, N. Singh, C. Galande, P. M. Ajayan, *Adv. Energy Mater.* **2015**, *5*, 1402115; c) B. Esser, F. Dolhem, M. Becuwe, P. Poizot, A. Vlad, D. Brandell, *J. Power Sources* **2021**, *482*, 228814; d) P. Poizot, J. Gaubicher, S. Renault, L. Dubois, Y. Liang, Y. Yao, *Chem. Rev.* **2020**, *120*, 6490; e) Y. Lu, Q. Zhang, F. Li, J. Chen, *Angew. Chem. Int. Ed.* **2022**, *61*, 2216047; f) W. Yan, J. Su, Z. M. Yang, S. Lv, Z. Jin, J. L. Zuo, *Small* **2021**, *17*, 2005209; g) W. Yan, F. Yu, Y. Jiang, J. Su, S.-W. Ke, Z. Tie, J.-L. Zuo, Z. Jin, *Small Structures* **2022**, *3*, 2200126.

[2] a) J. Calbo, M. J. Golomb, A. Walsh, *J. Mater. Chem. A* **2019**, *7*, 16571; b) C. Li, L. Liu, J. Kang, Y. Xiao, Y. Feng, F.-F. Cao, H. Zhang, *Energy Storage Mater.* **2020**, *31*, 115; c) R. Freund, O. Zaremba, G. Arnauts, R. Ameloot, G. Skorupskii, M. Dinca, A. Bavykina, J. Gascon, A. Ejsmont, J. Goscianska, M. Kalmutzki, U. Lachelt, E. Ploetz, C. S. Diercks, S. Wuttke, *Angew. Chem. Int. Ed.* **2021**, *60*, 23975; d) W. Yan, K. Fan, L.-M. Zheng, Z. Jin, *Small Structures* **2021**, *2*, 2100122; e) S. W. Ke, Y. Wang, J. Su, K. Liao, S. Lv, X. Song, T. Ma, S. Yuan, Z. Jin, J. L. Zuo, *J. Am. Chem. Soc.* **2022**, *144*, 8267.

[3] a) G. Férey, F. Millange, M. Morcrette, C. Serre, M.-L. Doublet, J.-M. Grenèche, J.-M. Tarascon, *Angew. Chem.* **2007**, *119*, 3323; b) A. Fateeva, P. Horcajada, T. Devic, C. Serre, J. Marrot, J.-M. Grenèche, M. Morcrette, J.-M. Tarascon, G. Maurin, G. Férey, *Eur. J. Inorg. Chem.* **2010**, 3789; c) S. Gu, Z. Bai, S. Majumder, B. Huang, G. Chen, *J. Power Sources* **2019**, *429*, 22.

[4] a) B. Tian, G. H. Ning, Q. Gao, L. M. Tan, W. Tang, Z. Chen, C. Su, K. P. Loh, *ACS Appl. Mater. Interfaces* **2016**, *8*, 31067; b) X. Lou, F. Geng, B. Hu, C. Li, M. Shen, B. Hu, *ACS Appl. Energ. Mater.* **2019**, *2*, 413.

[5] a) Q. Jiang, P. Xiong, J. Liu, Z. Xie, Q. Wang, X. Q. Yang, E. Hu, Y. Cao, J. Sun, Y. Xu, L. Chen, *Angew. Chem. Int. Ed.* **2020**, *59*, 5273; b) Z. Zhang, H. Yoshikawa, K. Awaga, *J. Am. Chem. Soc.* **2014**, *136*, 16112; c) Z. Zhang, H. Yoshikawa, K. Awaga, *Chem. Mater.* **2016**, *28*, 1298; d) M. E. Ziebel, C. A. Gaggioli, A. B. Turkiewicz, W. Ryu, L. Gagliardi, J. R. Long, *J. Am. Chem. Soc.* **2020**, *142*, 2653; e) Z. Peng, X. Yi, Z. Liu, J. Shang, D. Wang, *ACS Appl. Mater. Interfaces* **2016**, *8*, 14578.

[6] a) Q. Zhao, S. H. Li, R. L. Chai, X. Ren, C. Zhang, *ACS Appl. Mater. Interfaces* **2020**, *12*, 7504; b) C. A. Peeples, D. Kober, F. J. Schmitt, P. Tholen, K. Siemensmeyer, Q. Halldorson, B. Çoşut, A. Gurlo, A. O. Yazaydin, G. Hanna, G. Yücesan, *Adv. Funct. Mater.* **2021**, *31*, 2007294; c) L. Yang, M. Dinca, *Angew. Chem. Int. Ed.* **2021**, *60*, 23784; d) J. Wang, X. Guo, P. Apostol, X. Liu, K. Robeyns, L. Gence, C. Morari, J.-F. Gohy, A. Vlad, *Energy Environ. Sci.* **2022**, *15*, 3923; e) D. Rambabu, A. E. Lakraychi, J. Wang, L. Sieuw, D. Gupta, P. Apostol, G. Chanteux, T. Goossens, K. Robeyns, A. Vlad, *J. Am. Chem. Soc.* **2021**, *143*, 11641; f) L. Kong, M. Liu, H. Huang, Y. Xu, X. H. Bu, *Adv. Energy Mater.* **2022**, *12*, 2100172; g) R. C. K. Reddy, X. Lin, A. Zeb, C.-Y. Su, *Electrochem. Energy Rev.* **2022**, *5*, 312.

[7] a) J. H. Dou, L. Sun, Y. Ge, W. Li, C. H. Hendon, J. Li, S. Gul, J. Yano, E. A. Stach, M. Dinca, *J. Am. Chem. Soc.* **2017**, *139*, 13608; b) S. S. Park, Y. Tulchinsky, M. Dinca, *J. Am. Chem.*

Soc. **2017**, *139*, 13260; c) E. M. Miner, S. S. Park, M. Dinca, *J. Am. Chem. Soc.* **2019**, *141*, 4422.
[8] a) T. Chen, J. H. Dou, L. Yang, C. Sun, N. J. Libretto, G. Skorupskii, J. T. Miller, M. Dinca, *J. Am. Chem. Soc.* **2020**, *142*, 12367; b) L. S. Xie, S. S. Park, M. J. Chmielewski, H. Liu, R. A. Kharod, L. Yang, M. G. Campbell, M. Dinca, *Angew. Chem. Int. Ed.* **2020**, *59*, 19623; c) J. Liu, X. Song, T. Zhang, S. Liu, H. Wen, L. Chen, *Angew. Chem. Int. Ed.* **2021**, *60*, 5612; d) M. Wang, R. Dong, X. Feng, *Chem. Soc. Rev.* **2021**, *50*, 2764.
[9] M. Sadakiyo, H. Kitagawa, *Dalton Trans.* **2021**, *50*, 5385.
[10] B. M. Wiers, M. L. Foo, N. P. Balsara, J. R. Long, *J. Am. Chem. Soc.* **2011**, *133*, 14522.
[11] W. Xu, X. Pei, C. S. Diercks, H. Lyu, Z. Ji, O. M. Yaghi, *J. Am. Chem. Soc.* **2019**, *141*, 17522.
[12] a) L. S. Xie, G. Skorupskii, M. Dinca, *Chem. Rev.* **2020**, *120*, 8536; b) W. Xue, C. D. Sewell, Q. Zhou, Z. Lin, *Angew. Chem. Int. Ed.* **2022**, *61*, e202206512; c) R. A. Kharod, J. L. Andrews, M. Dincă, *Annu. Rev. Mater. Res.* **2022**, *52*, 103; d) S. Dutta, Y. D. More, S. Fajal, W. Mandal, G. K. Dam, S. K. Ghosh, *Chem. Commun.* **2022**, *58*, 13676.
[13] N. Kamaya, K. Homma, Y. Yamakawa, M. Hirayama, R. Kanno, M. Yonemura, T. Kamiyama, Y. Kato, S. Hama, K. Kawamoto, A. Mitsui, *Nat. Mater.* **2011**, *10*, 682.
[14] D. Di Stefano, A. Miglio, K. Robeyns, Y. Filinchuk, M. Lechartier, A. Senyshyn, H. Ishida, S. Spannenberger, D. Prutsch, S. Lunghammer, D. Rettenwander, M. Wilkening, B. Roling, Y. Kato, G. Hautier, *Chem* **2019**, *5*, 2450.
[15] A. Jouhara, N. Dupre, A. C. Gaillot, D. Guyomard, F. Dolhem, P. Poizot, *Nat. Commun.* **2018**, *9*, 4401.
[16] J. Liang, G. K. H. Shimizu, *Inorg. Chem.* **2007**, *46*, 10449.
[17] R. Pallach, J. Keupp, K. Terlinden, L. Frentzel-Beyme, M. Kloss, A. Machalica, J. Kotschy, S. K. Vasa, P. A. Chater, C. Sternemann, M. T. Wharmby, R. Linser, R. Schmid, S. Henke, *Nat. Commun.* **2021**, *12*, 4097.
[18] a) Z. Li, Z.-W. Liu, Z.-J. Mu, C. Cao, Z. Li, T.-X. Wang, Y. Li, X. Ding, B.-H. Han, W. Feng, *Mater. Chem. Front.* **2020**, *4*, 1164; b) T. Wei, Z. Wang, Q. Zhang, Y. Zhou, C. Sun, M. Wang, Y. Liu, S. Wang, Z. Yu, X. Qiu, S. Xu, S. Qin, *CrystEngComm* **2022**, *24*, 5014.
[19] V. Nozari, C. Calahoo, J. M. Tuffnell, P. Adelhelm, K. Wondraczek, S. E. Dutton, T. D. Bennett, L. Wondraczek, *Sci. Rep.* **2020**, *10*, 3532.
[20] C. Yu, J. H. He, J. M. Lu, *Small* **2022**, *18*, 2204023.
[21] a) R. G. Franz, *AAPS PharmSci* **2001**, *3*, 10; b) C. M. Sevrain, M. Berchel, H. Couthon, P. A. Jaffres, *Beilstein J. Org. Chem.* **2017**, *13*, 2186.

Manuscript received: July 14, 2023
Accepted manuscript online: August 31, 2023
Version of record online: September 13, 2023